Direct path integral estimators for isotope fractionation ratios

Bingqing Cheng[1] and Michele Ceriotti[1]

[1] *Laboratory of Computational Science and Modeling, École Polytechnique Fédérale de Lausanne, 1015 Lausanne, Switzerland*

Fractionation of isotopes among distinct molecules or phases is a quantum effect which is often exploited to obtain insights on reaction mechanisms, biochemical, geochemical and atmospheric phenomena. Accurate evaluation of isotope ratios in atomistic simulations is challenging, because one needs to perform a thermodynamic integration with respect to the isotope mass, along with time-consuming path integral calculations. By re-formulating the problem as a particle exchange in the ring polymer partition function, we derive new estimators giving direct access to the differential partitioning of isotopes, which can simplify the calculations by avoiding thermodynamic integration. We demonstrate the efficiency of these estimators by applying them to investigate the isotope fractionation ratios in the gas-phase Zundel cation, and in a few simple hydrocarbons.

arXiv:1412.1308v1 [physics.chem-ph] 3 Dec 2014

I. INTRODUCTION

There is little doubt that modelling explicitly the behavior of electrons requires a quantum mechanical treatment. The nuclei of atoms, on the other hand, are typically treated as classical point particles in atomistic simulations. In many cases – most notably for the lighter elements – the quantum nature of the nuclei gives rise to significant physical effects even at room temperature or above. Examples are the large deviations from the Dulong-Petit limit of the heat capacity of solids, the large isotope kinetic effects that are often observed in reactions that involve a hydrogen transfer as the rate-limiting step [1], and the deviations of the particle momentum distribution of nuclei from the Maxwell-Boltzmann predictions [2].

One of the most evident signs of the quantum nature of light nuclei is the fractionation of two isotopes X and X′ between two environments A and B – where the two environments could correspond to different thermodynamic phases, different compounds or inequivalent positions in the same molecule

$$\mathrm{X_A} + \mathrm{X'_B} \overset{\Delta G}{\rightleftharpoons} \mathrm{X_B} + \mathrm{X'_A}. \tag{1}$$

The isotope fractionation free energy ΔG would be zero if the nuclei behaved classically[3]. Owing to the quantum nature of the X nuclei, instead, it takes on a finite and measurable value which often depends strongly on the temperature T or the pressure. Isotope fractionation is usually characterized in terms of the fractionation ratio $\alpha_{\text{A-B}} = \exp(-\beta \Delta G_{\text{A-B}})$ at the inverse temperature $\beta = 1/k_B T$. Since $\alpha_{\text{A-B}}$ is usually quite close to unity, it is customary to express the fractionation ratio in the form $1000 \ln(\alpha_{\text{A-B}})$, and we adopt this convention here.

The isotope fractionation ratio can be determined experimentally with exquisite precision, and is used routinely to gain insight into reactions and phase transformations in geochemistry, biology and atmospheric sciences [4]. For instance, isotope fractionation can be used to trace the origin of water in clouds [5], or to reconstruct paleoclymatic records [6] and even to characterize the origin of wine [7]. When comparing experimentally-determined fractionation ratios with simulations, one has to distinguish between equilibrium isotope fractionation – the ratio that is reached after the different phases involved have reached thermodynamic equilibrium, and which is due exclusively to the quantum nature of the isotopes involved – and so-called kinetic isotope effects – that are due to the fact that differences in isotope mass affect reaction rates both classically and quantum mechanically, and that can lead to accumulation of one isotope in a non-equilibrium process [8]. Here we will focus on the computational determination of *equilibrium* isotope fractionation, so our results can be directly compared with experiments only in systems where thermodynamic equilibrium has been reached. However, accurate theoretical determination of the equilibrium isotope ratio is also useful to set an absolute reference for the equilibrium ratio, which can help determining the kinetic factors that contribute to the observed fractionation.

Evaluating fractionation ratios from simulations is far from trivial, because of the need of modelling accurately nuclear quantum effects (NQEs). For small gas-phase molecules, one often computes an approximate quantum mechanical partition function based on harmonic vibrations and rigid rotations [9]. However, the harmonic approximations do not allow one to reach an accuracy on par with the experimental techniques [10, 11], and cannot be applied to the condensed phase. Molecular dynamics combined with a path integral formalism [12–14] provides an accurate but computationally demanding approach to fully account for the quantum nature of the nuclei.

The conventional approach to compute the exact fractionation ratio in path integral molecular dynamics simulations involves performing a thermodynamic integration of the mean quantum kinetic energy of the tagged atom $\langle T \rangle$ as a function of the isotope mass [8]

$$-\beta \ln(\alpha_{\text{A-B}}) = \Delta G_{\text{A-B}} = \int_m^{m'} \frac{\langle T \rangle_{\text{B},\mu}}{\mu} - \frac{\langle T \rangle_{\text{A},\mu}}{\mu} \mathrm{d}\mu. \tag{2}$$

Many improvements have been proposed based on this scheme, including employing a change of variables to reduce the number of thermodynamic integration points, using re-weighting to compute the kinetic energy in a

substituted system out of a simulation with only the most abundant isotope [10], and using correlated-noise Langevin dynamics [15] or high-order path integral factorizations to accelerate the convergence with the number of replicas [16, 17].

Here we demonstrate that it is possible to evaluate the isotope fractionation ratios directly, without the need for a thermodynamic integration. The corresponding estimators are derived from the ratio of the partition functions of the isotope-substituted systems, which is obtained by a "virtual substitution" of the isotopes of the tagged atom. This procedure is closely related to the the free-energy perturbation estimators for the mass-scaled kinetic energy introduced in Ref. 10. Since it avoids the mass integration altogether it is more convenient, computationally advantageous, and immune to errors in the integral for the isotope mass.

The structure of this paper is as follows. We first introduce the theory underlying these direct fractionation estimators in Section II, then discuss their application to the Zundel cation in Section III, and to hydrocarbons in Section IV. Then, we finally draw our conclusions.

II. THEORY AND METHODS

A. The path integral partition function

Consider a system of N distinguishable particles described by the Cartesian Hamiltonian

$$H = \sum_{i=1}^{N} \frac{p_i^2}{2m_i} + V(q_1, \ldots, q_N), \tag{3}$$

and the corresponding quantum mechanical partition function

$$Z = \mathrm{Tr}\left[e^{-\beta \hat{H}}\right] \tag{4}$$

with $\beta = 1/k_{\mathrm{B}}T$. The imaginary-time path integral formalism [12–14] makes it possible to map the quantum mechanical partition function (4) onto the classical partition function

$$Z \simeq Z_P = \frac{1}{(2\pi\hbar)^{3NP}} \int d\mathbf{p} \int d\mathbf{q}\, e^{-\beta_P H_P(\mathbf{p},\mathbf{q})}, \tag{5}$$

where $\beta_P = \beta/P$.

The classical ring polymer Hamiltonian $H_P(\mathbf{p},\mathbf{q})$ describes P copies of the physical system with corresponding particles in adjacent replicas connected by harmonic springs:

$$H_P(\mathbf{p},\mathbf{q}) = K_P(\mathbf{p}) + V_P(\mathbf{q}) + S_P(\mathbf{q}), \tag{6}$$

where we introduced the classical kinetic energy

$$K_P(\mathbf{p}) = \sum_{i=1}^{N}\sum_{j=1}^{P} \frac{[p_i^{(j)}]^2}{2m_i}, \tag{7}$$

the sum of the potential energies of every replica

$$V_P(\mathbf{q}) = \sum_{j=1}^{P} V(q_1^{(j)}, \ldots, q_N^{(j)}), \tag{8}$$

and the spring energy

$$S_P(\mathbf{q}) \equiv \sum_{i=1}^{N} S(q_i, m_i) = \sum_{i=1}^{N}\sum_{j=1}^{P} \frac{1}{2} m_i \omega_P^2 [q_i^{(j)} - q_i^{(j-1)}]^2. \tag{9}$$

Here the harmonic spring frequency is $\omega_P = 1/\beta_P\hbar$, $q_i^{(j)}$ indicates the three dimensional Cartesian coordinates for the jth replica of the ith particle, and the cyclic boundary conditions $q_i^{(0)} \equiv q_i^{(P)}$ are implied. The ring-polymer partition function Z_P converges to the correct quantum mechanical result as $P \to \infty$. Note also that the momenta in Eq. (5) are only sampling devices, and can be integrated out trivially. In the following we will only consider the configurational ring polymer partition function

$$\bar{Q} = \int d\mathbf{q}\, e^{-\beta_P (S_P(\mathbf{q}) + V_P(\mathbf{q}))}, \tag{10}$$

where we omitted the P subscript and the constant prefactors for convenience of notation.

B. Direct estimators for isotope fractionation ratios

Assume, without loss of generality, that the Cartesian coordinates of an X atom are denoted by q_1. The partition function of system A containing the X isotope can be expressed as

$$\bar{Q}_{\mathrm{A}} = \int_{\mathrm{A}} d\mathbf{q}\, e^{-\beta_P V_{P,\mathrm{A}}(\mathbf{q})} e^{-\beta_P \sum_{i=2}^{N_{\mathrm{A}}} S(q_i, m_i)} e^{-\beta_P S(q_1, m)}, \tag{11}$$

where the integral is meant to extend over the configuration space of system A, and the contribution from the spring energy of the X atoms is singled out, taking into account that $m_1 = m$. $V_{P,\mathrm{A}}$ is the sum of the potential energy function V_{A} over the P path integral beads. The partition function $\bar{Q}'_{\mathrm{A}}$ for the system A where isotope X has been substituted by X$'$ can be easily obtained by making the change $m \leftarrow m'$. $\bar{Q}_{\mathrm{B}}$ and $\bar{Q}'_{\mathrm{B}}$ are the analogous expressions for the system B.

Let us consider the two phases as separated and non-interacting. This is always the case if one considers isotope substitution between bulk phases for which the interface between the two subsystems can be neglected, and a more general formulation that can be used when there is not a clear-cut distinction between the two states is discussed in Appendix A. Then, the combined partition function for X in A and X$'$ in B is just $\bar{Q}_{\mathrm{A}}\bar{Q}'_{\mathrm{B}}$. The relative probability of the two isotope configurations – which is precisely the fractionation ratio – is the ratio of the

combined partition functions

$$\alpha_{A-B} = \frac{\bar{Q}'_{\rm A}\bar{Q}_{\rm B}}{\bar{Q}_{\rm A}\bar{Q}'_{\rm B}}. \quad (12)$$

Direct thermodynamic estimator for the isotope fractionation ratio. Now consider $\bar{Q}'_{\rm A}/\bar{Q}_{\rm A}$, which reads

$$\frac{\int_A d\mathbf{q}\, e^{-\beta_P V_P(\mathbf{q})} e^{-\beta_P \sum_{i=2}^N S(q_i,m_i)} e^{-\beta_P S(q_1,m')}}{\int_A d\mathbf{q}\, e^{-\beta_P V_P(\mathbf{q})} e^{-\beta_P \sum_{i=2}^N S(q_i,m_i)} e^{-\beta_P S(q_1,m)}}. \quad (13)$$

By multiplying and dividing the integrand at the numerator by $e^{-\beta_P S(q_1,m)}$, one sees that (13) is just the ensemble average of the direct thermodynamic estimator

$$\mathcal{Z}^{\rm TD}_{m,m'} \equiv \exp\left[-\frac{1}{2}\beta_P\omega_P^2(m'-m)\sum_{j=1}^{P}[q_1^{(j)} - q_1^{(j+1)}]^2\right] \quad (14)$$

over a simulation of system A containing the isotope X of mass m, i.e.

$$\frac{\bar{Q}'_{\rm A}}{\bar{Q}_{\rm A}} = \left\langle \mathcal{Z}^{\rm TD}_{m,m'} \right\rangle_{{\rm A},m}. \quad (15)$$

Note that when there are multiple equivalent X atoms in the system it is possible to improve the statistical convergence of the estimator by averaging the values of $\mathcal{Z}^{\rm TD}_{m,m'}$ computed separately for each equivalent atom.

In a similar way, one can obtain the ratio $\bar{Q}'_{\rm B}/\bar{Q}_{\rm B}$, as an average of $\mathcal{Z}^{\rm TD}_{m,m'}$ over a simulation of the system B, so that ultimately the fractionation ratio can be expressed as

$$\alpha^{\rm TD}_{A-B} = \frac{\left\langle \mathcal{Z}^{\rm TD}_{m,m'} \right\rangle_{{\rm A},m}}{\left\langle \mathcal{Z}^{\rm TD}_{m,m'} \right\rangle_{{\rm B},m}}. \quad (16)$$

In order to evaluate the isotope fractionation ratio between systems A and B, only *two* simulations need to be performed, containing only the naturally abundant isotope. Furthermore, the computation for each value of $\mathcal{Z}^{\rm TD}_{m,m'}$ is inexpensive, as it does not involve evaluating the physical potential but just the harmonic spring energy.

Connection with the free-energy perturbation estimators of the particle kinetic energy. This direct thermodynamic estimator is closely related to the thermodynamic free energy perturbed (i.e. re-weighted) (TD-FEP) kinetic energy estimator introduced in Ref. 10. Consider a "pure" thermodynamic version (in Ref. 10 the centroid-virial form $T_{\rm CV}(q) = \frac{1}{2\beta} + \frac{1}{2P}\sum_{j=1}^{P}\left(q^{(j)} - \bar{q}\right)\frac{\partial V}{\partial q^{(j)}}$ was used for the kinetic energy term)

$$\langle T_{\rm TD}\rangle^{\rm TD}_{\mu} = \frac{\langle T_{\rm TD}(\mu,q)\exp\left[-h_{\rm TD}(\mu,q)\right]\rangle_m}{\langle \exp\left[-h_{\rm TD}(\mu,q)\right]\rangle_m}, \quad (17)$$

with

$$T_{\rm TD}(\mu,q) = \frac{1}{2\beta_P} - \frac{1}{2P}\mu\omega_P^2\sum_{j=1}^{P}\left(q^{(j)} - q^{(j-1)}\right)^2, \quad (18)$$

and

$$h_{\rm TD}(\mu,q) = \frac{(\mu-m)\beta_P\omega_P^2}{2}\sum_{j=1}^{P}\left(q^{(j)} - q^{(j-1)}\right)^2. \quad (19)$$

Also, recall that in this context the fractionation ratio is obtained by performing a thermodynamic integration with respect to mass (Eq. (2)). It is then easy to see that Eq. (16) is equivalent to performing analytically the integral with respect to μ in (2) – for instance by noticing that $-\beta\frac{\partial}{\partial m'}\ln\left\langle \mathcal{Z}^{\rm TD}_{m,m'}\right\rangle_{{\rm A},m}$ and $\langle T_{\rm TD}\rangle^{\rm TD}_{{\rm A},m'}/m'$ differ only by an additive constant that cancels out when one combines the term for system B in Eq. (2).

In the light of this connection, one sees that the direct thermodynamic estimator (14) can be regarded as a simpler, more convenient form of the TD-FEP estimator. It can be used in all the cases in which a free-energy perturbation approach is applicable, and avoids altogether the need of integrating over different values of the scaled mass μ.

As discussed in Ref. 10, the large fluctuations in the exponent of the TD-FEP estimator for large changes in mass (which is effectively the same term appearing in Eq. (14)) lead to a dramatic degradation of the sampling performance, which can be recognized by the appearance of abrupt changes of the cumulative average during the course of a simulation. Averaging the direct estimator is not fully equivalent to a re-weighing procedure, so the results of Ref. 18 do not strictly apply. Still as we will see, the large fluctuations in the exponential, and their growth with the number of beads P make the use of Eq. (14) impractical at low temperature and/or for isotope mass ratios very different from one.

Direct scaled-coordinates estimator for the isotope fractionation ratio. To obtain a more favorable behavior of the statistical efficiency with large number of beads P and isotope mass ratio, we derived an alternative scaled-coordinates estimator $\mathcal{Z}^{\rm SC}_{m,m'}$. We consider again the ratio of partition functions $\bar{Q}'_{\rm A}/\bar{Q}_{\rm A}$ as in Eq. (13), and we apply the change of variables

$$q_1^{(j)} \leftarrow \overline{q}_1 + \sqrt{\frac{m'}{m}}\left(q_1^{(j)} - \overline{q}_1\right), \quad (20)$$

to the integral at the numerator. Here $\overline{q}_1 = \sum_j q_1^{(j)}/P$ is the position of the centroid, and the change of variables corresponds to a scaling of the ring polymer coordinates relative to the centroid [19]. With this transformation, the integral in the numerator of Eq. (13) can be written in the form

$$|J|\int_A d\mathbf{q}\, e^{-\beta_P V_P(\mathbf{q})} e^{-\beta_P\sum_{i=2}^N S(q_i,m_i)} e^{-\beta_P S(q_1,m)} \times e^{-\beta_P\left[\sum_{j=1}^P V(q_1'^{(j)},\ldots,q_N^{(j)}) - V(q_1^{(j)},\ldots,q_N^{(j)})\right]} \quad (21)$$

where $q_1'^{(j)} = \overline{q}_1 + \sqrt{\frac{m}{m'}}\left(q_1^{(j)} - \overline{q}_1\right)$, and the Jacobian $|J|$ takes a constant value. Performing analogous manipulations for $\bar{Q}'_B$ in $\bar{Q}'_B/\bar{Q}_B$, one sees that the isotope

fractionation ratio can be written as

$$\alpha^{\mathrm{SC}}_{A-B} = \frac{\left\langle \mathcal{Z}^{\mathrm{SC}}_{m,m'} \right\rangle_{A,m}}{\left\langle \mathcal{Z}^{\mathrm{SC}}_{m,m'} \right\rangle_{B,m}}, \tag{22}$$

where the Jacobians have cancelled out, and we have introduced a direct scaled-coordinates estimator

$$\mathcal{Z}^{\mathrm{SC}}_{m,m'} \equiv \exp\left[-\beta_P \sum_{j=1}^{P} V(q_1'^{(j)}, \ldots, q_N^{(j)}) - V(q_1^{(j)}, \ldots, q_N^{(j)}) \right], \tag{23}$$

that can be used in the same way as its $\mathcal{Z}^{\mathrm{TD}}_{m,m'}$ counterpart. Each evaluation of Eq. (23) requires computing the inter-atomic potential, so this estimator is not as inexpensive as the thermodynamic version. At low temperature or for large isotope mass ratios, however, the gain in statistical efficiency more than offsets the additional computational cost.

It is worth mentioning that also this estimator can be shown to correspond to an exact, analytical mass integration of the scaled-coordinates free energy perturbed kinetic energy estimator (i.e. SC-FEP) introduced in Ref. 10. Contrary to the case of $\mathcal{Z}^{\mathrm{TD}}_{m,m'}$, performing the integration analytically is more than a matter of practical convenience. Each evaluation of the SC-FEP estimator requires a separate calculation of the potential energy function, and so avoiding the thermodynamic integration not only reduces the computational cost, but also circumvents discretization error even in cases in which the smoothing of the integrand introduced in Ref. 10 is not effective. Furthermore, the evaluation of $\mathcal{Z}^{\mathrm{SC}}_{m,m'}$ does not require computing derivatives of V, which might be convenient in cases where the forces are not used for sampling, as it is the case in Monte Carlo path integral simulations.

In the above discussion, $\mathcal{Z}^{\mathrm{SC}}_{m,m'}$ is taken from the simulations of the most abundant isotope type, which seems like the obvious choice. However, in some circumstances, it might be advantageous to perform the backward substitution, by sampling from a simulation containing one atom of the rare isotope X′. As we will comment on in Section III, this is due to the fact that $\mathcal{Z}^{\mathrm{SC}}_{m',m}$ has better statistical properties for $m' > m$.

The functional form of the direct estimators described above is based on the primitive second-order Trotter expansion of the Boltzmann operator. The generalization to higher-order expansions is straightforward. The derivation of the direct estimators under the Takahashi–Imada scheme [20] is discussed in the Appendix B. As we will see in practical cases, applying the fourth-order correction may accelerate the convergence with respect to the number of beads P, but may also impact adversely the statistical efficiency of the estimators.

Another promising approach to reduce the number of path integral replicas needed for convergence is that of using correlated-noise Langevin dynamics [15]. In its current form, however, the path integral Generalized Langevin Equation (PIGLET) thermostat does not enforce the bead-bead correlations that are necessary to accelerate the convergence of complex estimators such as those introduced in the present work. In the specific case of the liquid-vapor fractionation in water, a coincidental cancellation of errors makes it possible to use free-energy perturbation estimators together with PIGLET [10, 21]. Unfortunately, in all the examples we tested here results were not reliable, so using this option should only be considered after careful testing. It is however worth mentioning that, by computing inexpensively the kinetic energy of isotopes, PIGLET techniques can be very useful when one prefers to use conventional thermodynamic integration, or when one simply wants to estimate roughly $\alpha_{\text{A-B}}$ based on the difference in kinetic energy between the two phases.

III. POSITION-SPECIFIC AND CLUMPED ISOTOPE RATIOS IN $H_5O_2^+$

The Zundel cation $H_5O_2^+$, together with the Eigen cation H_3O^+, is one of the limiting states that are used to rationalize the behavior of a solvated proton, and plays a crucial role in our understanding of proton transport [22] and the autoionization of water [23]. Extensive experimental [24–28] and theoretical [29–37] studies of an isolated Zundel cation in the gas phase have been conducted, most notably by means of vibrational spectroscopy [38, 39], to probe its structure and the extent of the coupling between its constituent atoms. In both experimental and computational studies, the H/D isotopic substitution were found to significantly affect the intensity of infrared peaks of mixed H/D species [40, 41]. One observes a clear preference for H to occupy the central position of the singly-deuterated Zundel ion – which can be qualitatively understood as the configuration that minimizes the total zero-point energy of the substituted molecule.

Simulation details We have evaluated quantitatively the position-dependent H/D fractionation ratio between the central and peripheral positions in the singly-deuterated Zundel cation $H_4DO_2^+$, as well as the clumped-isotope $^{16}O/^{18}O$ enrichment, which measures the propensity of rare isotopes to clump together. We used a high-accuracy potential energy surface fitted from CCSD(T) data [37], so our results should represent quantitative predictions that can be verified by spectroscopic measurements. We performed path integral molecular dynamics (PIMD) simulations at 300K, using the implementation of PIMD and of the direct fractionation estimators which are available in the i-PI code [42]. We used an efficient local path integral Langevin (PILE) thermostat with targeted optimal sampling on the internal

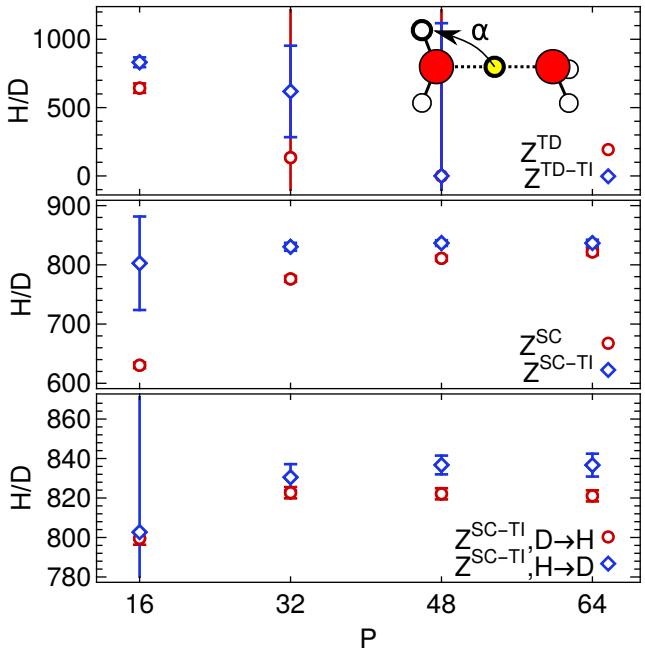

Figure 1. The position-specific isotope ratio $1000 \ln \alpha$ of H/D between a peripheral position and the central position in $H_2O \cdot H^+ \cdot OH_2$, as a function of the number of beads. Red, white and yellow spheres indicate O, H and D, respectively. The top panel reports the results for the thermodynamic estimator, the middle panel reports the scaled-coordinates estimators, and the bottom panel compares the results for forward H→D and backwards D→H substitution.

ring-polymer normal modes ($\gamma_k = \omega_k$) and a white-noise Langevin thermostat applied to the centroid, with a time constant of 1ps [43]. A time step of 0.25fs was used, and each simulation was run for 2×10^6 steps including the equilibration of 20,000 steps. We computed and output every four steps the direct estimators ($\mathcal{Z}^{\mathrm{TD}}_{m,m'}$ and $\mathcal{Z}^{\mathrm{SC}}_{m,m'}$) along with their fourth-order counterparts ($\mathcal{Z}^{\mathrm{TD\text{-}TI}}_{m,m'}$ and $\mathcal{Z}^{\mathrm{SC\text{-}TI}}_{m,m'}$, see Appendix B). In all cases we computed the estimators every 4 time steps and for a single instance of each atom kind, so as to be able to compare statistical efficiency in a straightforward manner. As we will discuss later, the efficiency of the TD estimator could be improved inexpensively by evaluating it more often and for all the statistically-equivalent atoms in the simulation.

Convergence and efficiency of the direct estimators for $H_5O_2^+$ Let us examine the convergence of the isotope fractionation ratios with respect to the number of beads for the Zundel ion, and compare critically the relative statistical efficiency of the various estimators that have been introduced in the present paper. Fig. 1 reports the isotope fractionation ratio for deuterium to substitute hydrogen at one of the peripheral positions comparing to the central "charged" position, with the equilibrium

$$H_2O \cdot D^+ \cdot OH_2 \overset{\Delta G}{\rightleftharpoons} DHO \cdot H^+ \cdot OH_2. \qquad (24)$$

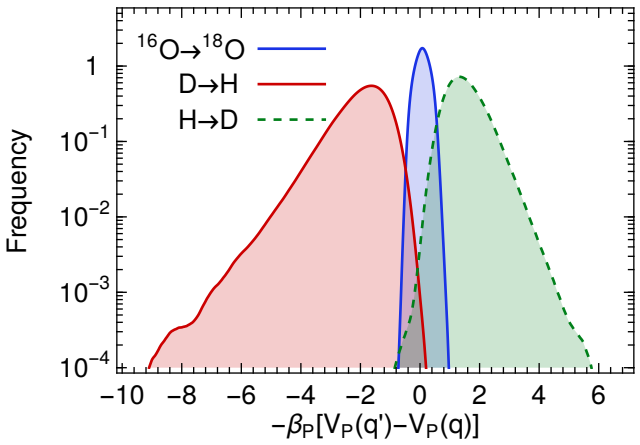

Figure 2. The frequency count for the argument of the exponential term entering the $\mathcal{Z}^{\mathrm{SC}}_{m,m'}$ estimator. The forward and backward H/D substitutions are compared, as well as the exchange of the two oxygen isotopes.

The upper panel uses the direct thermodynamic estimator (16), whose fluctuations increase with the number of beads. For any number of beads greater than 16, the statistical error on $\mathcal{Z}^{\mathrm{TD}}_{m,m'}$ is huge, making this estimator useless for determining H/D fractionation at room temperature or below. At $P = 64$, our best estimate using the thermodynamic estimator is completely outside of the range of the figure.

The middle panel reports the results from the direct scaled-coordinates estimator $\mathcal{Z}^{\mathrm{SC}}_{m,m'}$. In analogy with the centroid virial kinetic energy estimator T_{CV} [19] and the SC-FEP estimator [10], the fluctuations are independent on the number of beads. Using the primitive second-order Trotter formulation, 48 beads are needed to reduce the systematic error to about 3% in $1000 \ln \alpha$. The fourth-order Takahashi–Imada estimator ($\mathcal{Z}^{\mathrm{SC\text{-}TI}}_{m,m'}$, Eq. (B4)), accelerates substantially the convergence with respect to the number of beads, at the expense however of a larger statistical uncertainty for low numbers of beads due to the effect of the reweighing procedure [18].

The calculations discussed above were performed by computing direct estimators in a simulations of the $H_5O_2^+$ molecule, effectively performing the virtual substitution H → D for the central hydrogen atom, and one of the peripheral atoms. It is however also possible to evaluate the same quantities performing simulations of $DHO \cdot H^+ \cdot OH_2$ and $H_2O \cdot D^+ \cdot OH_2$, and computing the direct estimators for the virtual backward substitution D → H. The lower panel of Fig. 1 illustrates such results, which are affected by a considerably lower statistical error compared with the forward exchange H → D.

It is worth investigating in some detail for the reason why the substitution from higher to lower mass has better statistical properties. Following the discussion about the efficiency of the scaled-coordinates free-energy perturbation estimator in Ref. 10, the opposite

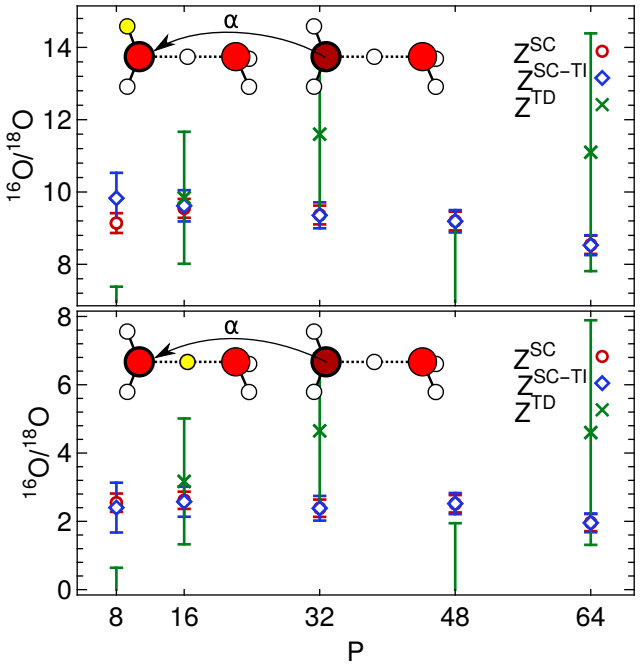

Figure 3. The clumped isotope ratio $1000 \ln \alpha$ of $^{16}O/^{18}O$ in the deuterated Zundel ion, as a function of the number of beads. The upper panel refers to the clumped ratio with $DHO \cdot H^+ \cdot OH_2$, while the lower panel considers the case of $H_2O \cdot D^+ \cdot OH_2$. ^{18}O is indicated by darker color, and D by bright yellow.

is expected: the fluctuations of the difference Hamiltonian $-\beta_P [V_P(q') - V_P(q)]$ are predicted to be larger for $D \to H$ than for $H \to D$ substitution. As shown in Figure 2, the distribution of the weights is indeed broader for the backward substitution. However, the weight distribution for $D \to H$ has a long non-Gaussian tail for negative values of $-\beta_P [V_P(q') - V_P(q)]$ so that a large fraction of configurations effectively contributes next to nothing to the accumulated average. Conversely, the distribution for the $H \to D$ case has a strongly non-Gaussian tail for *positive* values of $-\beta_P [V_P(q') - V_P(q)]$. Outliers in this direction will yield extremely large contributions to the average, despite occurring with very low probability. Each time a new outlier is encountered, it will dominate and shift dramatically the value of the cumulative average, which shows a characteristic zig-zag pattern and a slowly decaying statistical error. These observations highlight the importance of using extreme care when averaging exponentials, or performing re-weighing averages. While an analysis based on a Gaussian ansatz for the argument of the exponential allows one to assess qualitatively the "comfort zone" of applicability of a method [18], deviations from Gaussian statistics can have a dramatic impact on the quantitative accuracy of these predictions.

Simulations with the isotope-substituted species also made it possible to evaluate the clumped-isotope fractionation ratio for $^{16}O/^{18}O$. This corresponds to the enhanced probability of finding a rare isotope ^{18}O in a molecule that also contains deuterium rather than in $H_5O_2^+$, corresponding e.g. to the equilibrium

$$\begin{aligned} DHO \cdot H^+ \cdot OH_2 + H_2(^{18}O) \cdot H^+ \cdot OH_2 \overset{\Delta G}{\rightleftharpoons} \\ H_2O \cdot H^+ \cdot OH_2 + DH(^{18}O) \cdot H^+ \cdot OH_2. \end{aligned} \tag{25}$$

Fig. 3 shows the clumped isotope fractionation ratio corresponding to the equilibrium in Eq. (25), and the one corresponding to the alternative deuterium-substituted molecule $H_2O \cdot D^+ \cdot OH_2$. The ratio converges with number of beads more rapidly than for H/D, and has a considerably smaller statistical uncertainly. This can be easily explained considering the mass ratio associated $m(^{18}O)/m(^{16}O) = 1.1253$, which is much closer to unity than that of the H/D substitution. In the language of the free energy perturbation theory, the substitution between atoms with similar masses introduce a smaller perturbation, so that the original and the mutated systems have a larger overlap in phase space. For this reason, the statistical error on $\mathcal{Z}^{TD}_{m,m'}$ is not as unmanageable as in the case for H/D. Still, $\mathcal{Z}^{SC}_{m,m'}$ delivers a considerably better performance. As shown in Fig. 2, the bandwidth of the exponential term in $\mathcal{Z}^{SC}_{m,m'}$ is small, and so in the case of oxygen it is not necessary to resort to a backward substitution from the less abundant to the abundant isotope type.

The above analysis highlights the importance of considering carefully the statistical efficiency of different estimators when performing isotope-substitution simulations. For instance, we found that the statistical accuracy of thermodynamic estimators is catastrophic in the case of lighter atoms. The (relatively small) overhead of computing the scaled-coordinates estimator is more than compensated by the increase in statistical efficiency – particularly for small gas-phase molecules where one cannot exploit horizontal statistics. For the same reason, in the conditions that we considered in this example, it is more efficient to perform the backward $D \to H$ virtual substitution, while the in the case of heavier nuclei one should be able to use the more obvious substitution from the abundant to the rare isotope. For heavy isotopes, particularly when multiple equivalent atoms are present, or at high temperature, the thermodynamic estimator could become a more practical option. The discussion in Ref. 10 can give some guidelines as to whether one can use the thermodynamic estimator, or the scaled-coordinate version is to be preferred. Note however that, as we have shown, that analysis is only qualitative, because it disregards the non-Gaussian distribution of the scaled-coordinates difference Hamiltonian.

The Takahashi-Imada estimator $\mathcal{Z}^{SC\text{-}TI}_{m,m'}$ accelerates considerably the convergence with number of beads, without significantly affecting the sampling efficiency except for $P \leq 16$. With this choice, together with the $D \to H$ substitution, and considering the most converged simulation with $P = 64$, we computed the position-dependent H/D fractionation ratio $1000 \ln \alpha$ to be 821 ± 3

at $300K$. This means that the probability of finding a D atom at one of the peripheral sites is enhanced quantum-mechanically by a factor of 2.273 ± 0.006 compared to the central position. Considering also that there are four equivalent peripheral sites and just one central site, there is a more than 90% chance that a $DH_4O_2^+$ molecule will be observed in the $DHO \cdot H^+ \cdot OH_2$ configuration rather than as $H_2O \cdot D^+ \cdot OH_2$. Since we based our calculation on a very high-accuracy potential energy surface [37], we believe it should be possible to verify quantitatively this prediction by measuring experimentally the relative populations.

Using $\mathcal{Z}^{\text{SC-TI}}_{m,m'}$ and $P = 64$, we also predicted the clumped isotope fractionation ratios $1000 \ln \alpha$ for $^{16}O/^{18}O$ relative to the pure $H_5O_2^+$ to be 8.5 ± 0.3 in $DHO \cdot H^+ \cdot OH_2$ and 2.0 ± 0.3 in $H_2O \cdot D^+ \cdot OH_2$. Since the clumped isotope enrichment can also be determined [44] by mass spectrometry of isotopologues, these theoretical predictions are also amenable to experimental verification.

IV. ISOTOPE FRACTIONATION RATIOS IN HYDROCARBONS

The isotopic compositions of gaseous hydrocarbons are used routinely as indicators of their origin, maturity and generation mechanism [45, 46]. Besides, isotope ratios for hydrocarbons are used as a tool to monitor biodegradation [47], biosynthesis [48] and photosythesis [49]. Furthermore, they provide evidence for the reconstruction of the ancient biogeochemical history [50, 51]. In most cases, the accumulation of different carbon isotopes in plants is due to kinetic isotope effects, and so the ratios computed here – that only account for the equilibrium contribution – cannot be directly compared with observed ratios, but only provide a reference "baseline".

To demonstrate the application of direct estimators in this context, we evaluated the hydrogen and carbon fractionation ratios between a few small gas phase hydrocarbon molecules. We used the reactive empirical potential AIREBO to describe the interaction between the atoms, since it provides a generally applicable framework that could be easily extended to other hydrocarbons [52, 53]. The simulation details for our PIMD calculations were identical to those indicated in Section III.

The convergence of direct estimators for gas-phase hydrocarbons. To assess the convergence with respect to the number of beads, and to determine the optimal strategy to apply the direct estimators to the gas phase hydrocarbons, we started by evaluating the differential fractionation of isotopes between methane and ethene at 300K.

The corresponding chemical equilibrium can be written as, e.g.

$$CH_3D + C_2H_4 \overset{\Delta G}{\rightleftharpoons} CH_4 + C_2H_3D. \qquad (26)$$

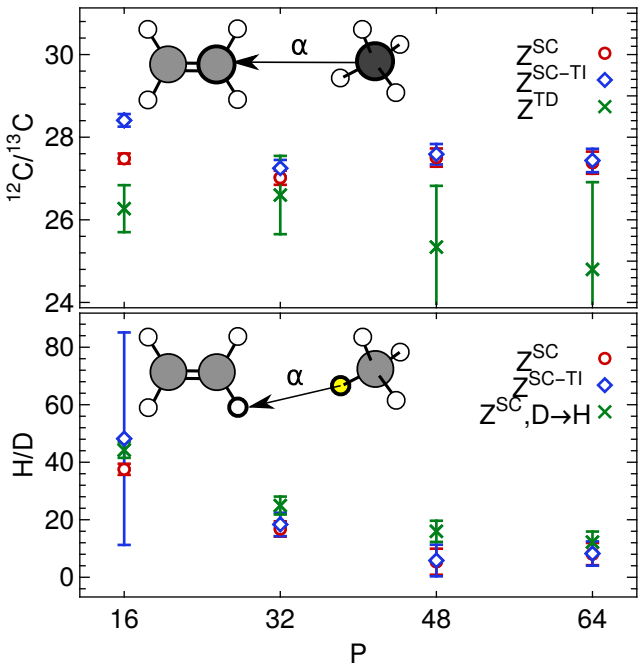

Figure 4. The isotope fractionation ratio $1000 \ln \alpha$ for $^{12}C/^{13}C$ and D/H between CH_4 and C_2H_4 as a function of the number of beads. Grey, dark grey and white spheres indicate ^{12}C, ^{13}C and H, respectively.

Fig. 4 demonstrates the convergence of fractionation ratio of carbon and hydrogen as a function of the number of beads. Result for carbon are already almost converged at $P = 16$, where the error of $\mathcal{Z}^{\text{TD}}_{m,m'}$ is still manageable, as the mass ratio $m(^{13}C)/m(^{12}C) = 1.083$ is very close to one. However, the much smaller error of $\mathcal{Z}^{\text{SC}}_{m,m'}$ means that in the absence of horizontal statistics the scaled-coordinate estimator is still the recommended choice. Convergence of H/D fractionation requires at least 48 beads when using the primitive second-order Trotter scheme. As observed in the case of the Zundel cation, performing the backward substitution $D \to H$ reduces noticeably the statistical error compared to the direct $H \to D$ substitution. In this case the the fourth-order Takahashi–Imada estimator ($\mathcal{Z}^{\text{SC-TI}}_{m,m'}$) does not lead to a significant improvement of convergence. As explained in Appendix C, this is due to a fortuitous cancellation of errors for the second-order estimators. Note also the very different scales of Fig. 4 and of Fig. 1: the fractionation ratio in the case of the Zundel cation is so large that a difference of 20 units of $1000 \ln \alpha$ is a small relative error, whereas in this case it amounts to 50% of $1000 \ln \alpha$. As we will see later, H/D fractionation between hydrocarbons involves a considerable degree of cancellation between different molecular directions, leading to an overall small value and apparently to a pronounced cancellation of errors when using Trotter estimators.

a. Simulation results and discussion Based on the convergence tests discussed above, we chose

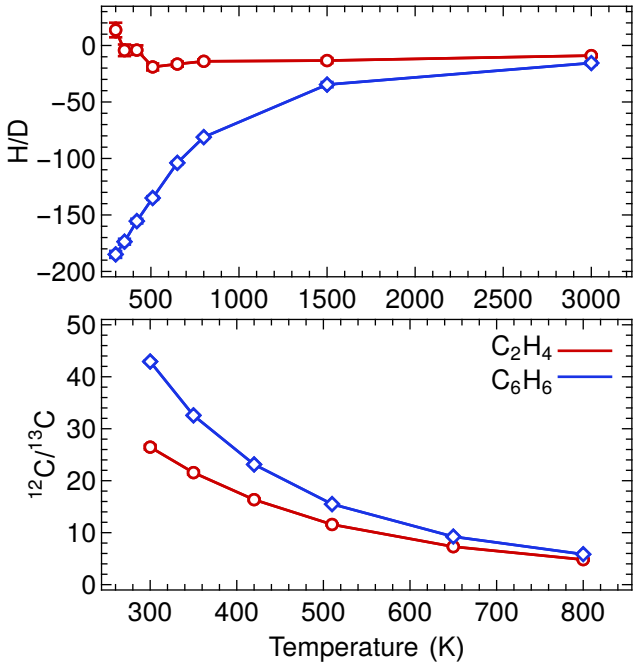

Figure 5. Quantum mechanical component of the H and C fractionation ratios between C_2H_4 and CH_4, and the ratios between C_6H_6 and CH_4. Notice the difference in the temperature scale.

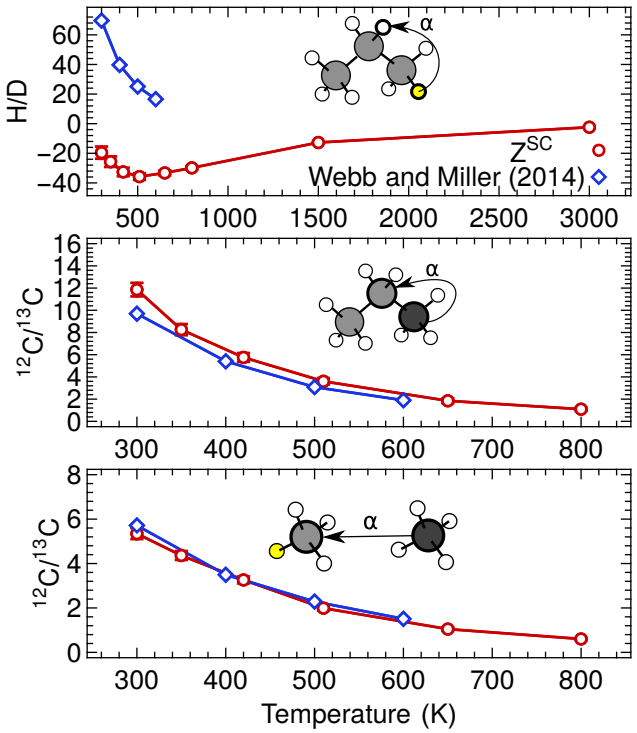

Figure 6. Upper and mid panel: position-specific H and C fractionation ratios in C_3H_8. Lower panel: clumped-isotopes C fractionation ratio in CH_3D. Notice the difference in the temperature scale.

to perform calculations with $P = 48$, using the scaled-coordinates estimator, and backward substitution to compute H/D fractionation. We performed simulations at different temperatures $T_i = \{300\text{K}, 350\text{K}, 420\text{K}, 510\text{K}, 650\text{K}, 800\text{K}\}$, using a parallel-tempering strategy to improve the statistical convergence [54].

We performed calculations for methane (CH_4), ethene (C_2H_4), benzene (C_6H_6), and will report all the fractionation ratios using methane as a reference. We also computed the clumped-isotope fractionation ratio for H/D and $^{12}C/^{13}C$ in methane, and the position-dependent isotope ratio in propane (C_3H_8).

Fig. 5 shows the fractionation ratio for C_2H_4 and C_6H_6 with reference to CH_4, corresponding to the chemical equilibrium in Eq. (26). ^{13}C has a preference for the molecule with the higher number of C–C bonds: even if carbon-carbon bonds have a lower content of zero-point energy than C–H bonds, the carbon atom shares a larger fraction of the zero-point energy, which qualitatively explains this trend. As the temperature increases, the fractionation ratio decreases monotonically to zero. The trend for H/D fractionation is not as straightforward. On one hand, deuterium has a strong preference for CH_4 relative to C_6H_6, that only approaches zero at very large temperatures. The ethene/methene fractionation ratio is much smaller, and shows an inversion between a preference for D to reside in ethene at low temperatures to a preference for methane at $T \gtrsim 400K$.

Before we comment on this inversion, let us consider the case of the position-specific ratios between the central CH_2 group and the methyl group in propane, for which temperature-dependent results are shown in the upper and middle panels of Fig. 6, and that correspond to the equilibria

$$\text{CH}_3 - \text{CH}_2 - \text{CH}_2\text{D} \overset{\Delta G}{\rightleftharpoons} \text{CH}_3 - \text{CHD} - \text{CH}_3 \qquad (27)$$

and

$$\text{CH}_3 - {}^{12}\text{CH}_2 - {}^{13}\text{CH}_3 \overset{\Delta G}{\rightleftharpoons} \text{CH}_3 - {}^{13}\text{CH}_2 - {}^{12}\text{CH}_3. \qquad (28)$$

In the lower panel of Fig. 6 we also report the clumped-isotope fractionation ratio for CH_3D, i.e.

$$^{13}\text{CH}_4 + \text{CH}_3\text{D} \overset{\Delta G}{\rightleftharpoons} \text{CH}_4 + {}^{13}\text{CH}_3\text{D}. \qquad (29)$$

The fractionation ratios for these reactions were also discussed in Ref. 11, where a traditional approach based on path-integral Monte Carlo simulations, and thermodynamic integration using 5 to 10 integration points were used, with a total of more than 2×10^{10} energy evaluations for each isotope substitution. The comparison is interesting because of the use of a different potential

energy surface: the calculations for methane in Ref. 11 were based on a a high-quality potential energy surface computed at the CCSD(T) level of theory [55], whereas the simulations for propane were based on the empirical CHARMM PES [56]. Fig. 6 also includes the results from Webb and Miller to illustrate the comparison.

In the cases involving $^{12}C/^{13}C$ fractionation, despite the very different potentials we employed, our results are both qualitatively and semi-quantitatively consistent with those of Ref. 11. ^{13}C has a higher affinity for the central methylene group in propane, and for the deuterated methane – both phenomena that can easily be explained in terms of the partitioning of zero-point energy between the atoms in different molecules.

In the case of H/D fractionation within propane, instead, our calculations give results that are qualitatively at odds with those of Ref. 11. Results based on the CHARMM force field show preference for deuterium to localize in the methyl groups and a monothonic dependence on temperature, whereas results based on AIREBO show preference for methylene, and a non-monothonic dependence that suggests there would probably be an inversion for $T < 300$K. Inversion in fractionation ratios as a function of temperature is observed in the liquid/vapor equilibra for water [21, 57], and is consistent with competing quantum effects between the changes of quantum kinetic energy along different molecular axes. For instance, if the change in the frequencies of the stretching and bending modes between two molecules have different sign, the isotope preference might change as the temperature is increased, since the effect from the lower-frequency mode will become negligible at lower temperature. These kinds of cancellations are more likely to occur for light atoms, for which there is larger anisotropy between the different components of the kinetic energy. It is therefore much harder to capture the qualitative fractionation behavior for light atoms than it is for the heavier isotopes, which reinforces the idea of using H/D isotope fractionation as a sensitive benchmark of different potential energy surfaces [21].

The above results show the differential fractionation between a number of gas-phase hydrocarbon molecules under thermodynamic equilibrium, and its strong temperature dependence. For natural gas there is a general trend for ^{13}C to be depleted in the lighter hydrocarbons [46], which is consistent with our calculations. However, because of the complicated chemical and biological processes involved during the natural gas production, it is not reasonable to make a direct comparison. Theoretical calculations based on more accurate potential energy surfaces can set an absolute reference point under the equilibrium conditions, so that the kinetic isotope effects can be singled out in the complicated natural gas generation processes.

V. DISCUSSION AND CONCLUSIONS

In this paper we have introduced two direct estimators of the isotope fractionation ratio, that were obtained by computing the ratio of the partition functions of the original and isotope-substituted systems. These estimators are closely related to those that have been recently introduced based on a free energy perturbation approach [10], and therefore their statistical efficiency is largely determined by the degree of the phase-space overlap between the original and the substituted systems. Hence, the statistical efficiency of these direct estimators is more favorable when the mass ratio between the isotopes approaches one, or when the system temperature increases so that the nuclear quantum effects get smaller.

In both benchmark applications considered here – the Zundel cation at 300K, and gas-phase hydrocarbons at room temperature and above – the scaled-coordinates version gave consistently better performance than the direct thermodynamic estimator, so that the small additional cost associated with the (relatively infrequent) evaluation of $\mathcal{Z}^{\mathrm{SC}}_{m,m'}$ is more than compensated. On the other hand, $\mathcal{Z}^{\mathrm{TD}}_{m,m'}$ can be evaluated almost for free, and so it is advisable to calculate it regardless, to provide cross-validation of results. When there are many equivalent substitution sites in the system, (e.g. a bulk liquid) it is possible to compute the estimator simultaneously for each site and exploit the horizontal statistics. In these cases, particularly for heavy isotopes and temperatures above 300K, $\mathcal{Z}^{\mathrm{TD}}_{m,m'}$ can be computed for all sites inexpensively, whereas $\mathcal{Z}^{\mathrm{SC}}_{m,m'}$ requires a separate potential energy evaluation for each site, which might tip the balance in favor of the thermodynamic version of our estimators.

In the case of the H/D substitution, we observed that for $\mathcal{Z}^{\mathrm{SC}}_{m,m'}$ performing the forward substitution from the lighter to the heavier isotope resulted in larger statistical errors than doing the backwards D→H substitution. The analysis in Ref. 10, which was based on a Gaussian ansatz for the free-energy perturbation weighing factor, gives the opposite prediction. We could explain this discrepancy based on the skewed, asymmetric distribution of the exponent in $\mathcal{Z}^{\mathrm{SC}}_{m,m'}$ (Fig. 2). The implications of this observation are relevant to a much broader class of problems than those considered in the present work: similar exponential terms also enter other methods based on statistical reweighing, such as biased molecular dynamics, Jarzynski's inequality, etc. Considering the shape of the distribution of the exponential term can help refine the predictions based on the estimate of its fluctuations, and increase the range of applicability of reweighing techniques.

When considering methods to accelerate the convergence of these estimators we found that unfortunately the combination of path integrals and generalized Langevin dynamics [15], that is very effective for the evaluation of NQEs on structural properties and kinetic energies,

does not help in the efficient evaluations of these estimators, that have a complex non-linear functional form and therefore depend on several bead-bead correlations that are not currently included in PI+GLE methods. However, we found that fourth-order direct estimator ($\mathcal{Z}^{\text{SC-TI}}_{m,m'}$) based on the Takahashi–Imada factorization can be computed quite easily, and they typically lead to improved convergence – even though in the case of hydrocarbons a fortuitous cancellation of errors made second-order estimators as efficient as those including the TI corrections. Since the evaluation of the terms needed in the TI scheme is completely inexpensive in case where forces are already computed to integrate the path integral dynamics, one should always compute them and assess on a case-by-case basis if the improved convergence compensates for the statistical errors associated with fourth-order methods.

The applications we have presented also allowed us to draw some observations about the isotope-fractionation behavior in the case of the Zundel cation and of gas-phase hydrocarbons. In H_4DO^+ one observes a very strong preference for hydrogen to reside in the central, shared position. These findings are consistent with prior experimental and theoretical work, and it would be possible to verify them quantitatively. Such a strong fractionation ratio also suggests that the temperature dependence of $\alpha_{\text{A-B}}$ could be used to assess the temperature of charged water clusters, similarly to what was recently proposed for neutral ones [58]. Fractionation in hydrocarbons shows relatively predictable trends in the case of $^{12}C/^{13}C$, with the heavier carbon isotope residing preferentially in the molecule or position with the largest number of C-C bonds. Comparison with previous results showed that this fractionation ratio is not very sensitive to the choice of inter-atomic potential. On the contrary, results for H/D fractionation showed qualitative discrepancies with previous work. This discrepancy can be traced to the fact that light elements often show a strongly anisotropic kinetic energy tensor, with different components that can change in opposite directions when changing the atom's environment. Since the value of $\alpha_{\text{A-B}}$ depends on a subtle cancellation between different components, it will then be more sensitive to the details of the potential, and possibly have a non-trivial temperature dependence.

The direct estimators we have introduced have been implemented in the development version of the path-integral interface i-PI[42], making them available for use together with a number of empirical forcefields and electronic structure software packages, including LAMMPS[59], CP2K[60] and FHI-AIMS[61]. Fourth-order corrections based on the Takahashi-Imada scheme can also be easily incorporated, accelerating the convergence with respect to the number of beads. These direct estimators can be regarded as the final step in the process of making the path integral evaluation of isotope fractionation ratios easily accessible, by eliminating altogether the need of performing a thermodynamic integration. They will allow a more widespread use of computational modelling to provide reference equilibrium ratios, and assist the interpretation of fractionation data in geochemistry, biology and atmospheric sciences.

Appendix A: Isotope fractionation in a fluxional setting

In the main text we have discussed the case of fractionation of isotopes between distinct phases, compounds, or molecular sites. Now, let us consider how the direct estimators can be used in a setting in which one cannot define a clear-cut distinction between the A and B states, but has just one system described by a potential V, and the two states are different regions of configuration space, that are associated to two characteristic functions $\theta_{\text{A}}(\mathbf{q})$ and $\theta_{\text{B}}(\mathbf{q})$, which are one if the configuration can be ascribed to one of the states, and zero otherwise. For instance, the functions could select configurations in which the tagged atom is at a given distance from an interface [62], or in a specific hydrogen-bonding environment.

The probability of finding the isotope X in state A is then given by

$$\rho_{\text{A}} = \frac{1}{P\bar{Q}} \int d\mathbf{q} \left[\sum_j \theta_{\text{A}}(q_1^{(j)}, \dots, q_N^{(j)}) e^{-\beta_P V_P(\mathbf{q})} e^{-\beta_P \sum_{i=2}^N S(q_i, m_i)} e^{-\beta_P S(q_1, m)} \right], \tag{A1}$$

and the probability of finding the isotope X′ in state B is

$$\rho'_{\text{B}} = \frac{1}{P\bar{Q}'} \int d\mathbf{q} \left[\sum_j \theta_{\text{B}}(q_1^{(j)}, \dots, q_N^{(j)}) e^{-\beta_P V_P(\mathbf{q})} e^{-\beta_P \sum_{i=2}^N S(q_i, m_i)} e^{-\beta_P S(q_1, m')} \right]. \tag{A2}$$

One quickly sees that the fractionation ratio can be written as $\rho'_{\text{A}}\rho_{\text{B}}/\rho_{\text{A}}\rho'_{\text{B}}$, so one is led to evaluate the ratio $\rho'_{\text{A}}/\rho_{\text{A}}$, which can be written as

$$\rho'_{\text{A}}/\rho_{\text{A}} = \langle \theta_{\text{A}} \mathcal{Z}_{m,m'} \rangle_m \,/\, \langle \theta_{\text{A}} \rangle_m \,. \tag{A3}$$

The ratio can be evaluated by performing a simulation of the abundant isotope X, and averaging $\mathcal{Z}_{m,m'}$ selectively over the configurations that are identified as A structures. One can compute $\rho'_{\text{B}}/\rho_{\text{B}}$ in a similar way, finally obtaining the desired fractionation ratio.

Appendix B: The fourth order direct estimators using the Takahashi–Imada factorization

The convergence of path integral simulations with the number of replicas can be accelerated by using a

high-order factorization of the Boltzmann operator $e^{-\beta\hat{H}}$ rather than the simple Trotter factorization that leads to Eq. (5). Many different high-order schemes have been proposed, and here we will focus on the Takahashi-Imada factorization [20], that leads to a partition function with an error term $\mathcal{O}(\beta_P^4)$, consistent with the Hamiltonian

$$H_{\rm TI}(\mathbf{p},\mathbf{q}) = K_P(\mathbf{p}) + V_P(\mathbf{q}) + S_P(\mathbf{q}) + V_{\rm TI}(\mathbf{q}) \quad \text{(B1)}$$

which contains a correction term that depends on the squared force

$$V_{\rm TI}(\mathbf{q}) = \frac{1}{24\omega_P^2}\sum_{i=1}^{N}\sum_{j=1}^{P}\frac{1}{m_i}\left(\frac{\partial V(q_1^{(j)},\ldots,q_N^{(j)})}{\partial q_i^{(j)}}\right)^2. \quad \text{(B2)}$$

The fourth-order direct estimators can then be obtained as

$$\mathcal{Z}^{\text{TD-TI}}_{m,m'} \equiv \exp\left[-\frac{\beta_P}{24\omega_P^2}\left(\frac{1}{m'}-\frac{1}{m}\right)\sum_{j=1}^{P}\left(\frac{\partial V(q_1^{(j)},\ldots,q_N^{(j)})}{\partial q_1^{(j)}}\right)^2 - \frac{1}{2}\beta_P\omega_P^2(m'-m)\sum_{j=1}^{P}[q_1^{(j)}-q_1^{(j+1)}]^2\right], \quad \text{(B3)}$$

and

$$\mathcal{Z}^{\text{SC-TI}}_{m,m'} \equiv \exp\left[-\beta_P\left(V_{\rm TI}(q_1',\ldots,q_N)-V_{\rm TI}(q_1,\ldots,q_N)\right) - \beta_P\sum_{j=1}^{P}V(q_1'^{(j)},\ldots,q_N^{(j)})-V(q_1^{(j)},\ldots,q_N^{(j)})\right]. \quad \text{(B4)}$$

Performing PIMD based on the Hamiltonian in Eq. (B1) would be impractical, as the corresponding forces contain terms that depend on the second derivatives of the physical potential. In practice, one typically uses a free-energy perturbation strategy to obtain averages consistent with Eq. (B1), while performing sampling based on the second-order partition function in Eq. (5) [17, 18, 63]. This entails treating $V_{\rm TI}$ as a small pertubation to the Trotter Hamiltonian in Eq. (6), and later recovering the fourth-order statistics by re-weighting configurations with the weight

$$w_{\rm TI}(\mathbf{q}) = e^{-\beta_P V_{\rm TI}(\mathbf{q})} \quad \text{(B5)}$$

so that for instance one can compute

$$\alpha^{\text{SC-TI}}_{A-B} = \frac{\left\langle \mathcal{Z}^{\text{SC-TI}}_{m,m'} w_{\rm TI}(\mathbf{q})\right\rangle_{(2),A,m} / \left\langle w_{\rm TI}(\mathbf{q})\right\rangle_{(2),A,m}}{\left\langle \mathcal{Z}^{\text{SC-TI}}_{m,m'} w_{\rm TI}(\mathbf{q})\right\rangle_{(2),B,m} / \left\langle w_{\rm TI}(\mathbf{q})\right\rangle_{(2),B,m}}. \quad \text{(B6)}$$

Note that the performance of reweighed high-order factorizations degrades as the size of the system being studied increases [18]. However, we noticed that the Takahashi–Imada factorization yields smaller fluctuations of the logarithm of the reweighing factors compared to the Suzuki-Chin factorization that was used in the analysis in Ref. [18], which can marginally extend the range of applicability of this approach.

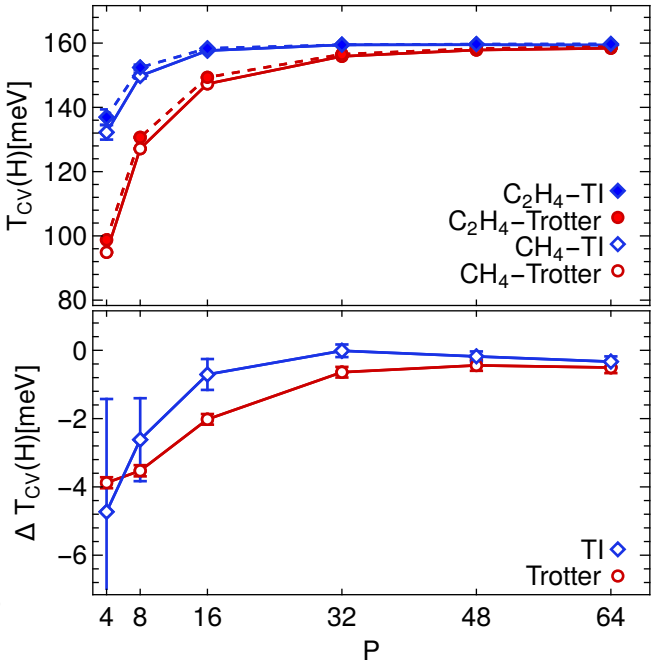

Figure 7. $T_{\rm CV}$ for CH_4 and C_2H_4, and $\Delta T_{\rm CV} = T_{\rm CV}^{\rm CH_4} - T_{\rm CV}^{\rm C_2H_4}$, as a function of the number of beads. The lines are provided only as aids for the eye.

Appendix C: Convergence of fourth order estimators for hydrogen isotopes fractionation between methane and ethene

Contrary to what we observed in the case of $H_5O_2^+$, the fourth-order Takahashi–Imada estimator ($\mathcal{Z}^{\text{SC-TI}}_{m,m'}$) does not lead to a significant improvement of the convergence with the number of beads. To understand why, we computed the effect of the Takahashi–Imada correction on the centroid viral kinetic energy[17] $T_{\rm CV}$ for CH_4 and C_2H_4, as well as on their difference $\Delta T_{\rm CV}$ (Fig. 7) – which to a first approximation is proportional to the isotope-substitution free energy [10]. Note that $T_{\rm CV}$ is far from converged with $P < 48$, and the TI correction does enhance its convergence considerably. However, when it comes to computing $\Delta T_{\rm CV}$, the errors in the Trotter estimate of kinetic energy for the two molecules largely cancel out, so that there is little or no improvement when considering the TI correction to $\Delta T_{\rm CV}$.

[1] Y. P. Liu, D. H. Lu, A. Gonzalez-Lafont, D. G. Truhlar, and B. C. Garrett, Journal of the American Chemical Society **115**, 7806 (1993).

[2] C. Andreani, D. Colognesi, J. Mayers, G. F. Reiter, and R. Senesi, Adv. Phys. **54**, 377 (2005).

[3] Note that in cases where the A and B systems contain a different number of equivalent positions that can be occupied by the minority isotope (e.g. consider HOD versus CH_3D), the equilibrium (1) also involves a component of configurational entropy, that means that *also classically* $\alpha_{\text{A-B}} \neq 0$. Here, unless otherwise specified, we will consider the equilibrium between two specified positions, i.e. we will write $\alpha_{\text{A-B}}$ to indicate the sole quantum mechanical component to fractionation $\alpha^{\text{tot}}_{\text{A-B}}/\alpha^{\text{class}}_{\text{A-B}}$.

[4] R. A. Werner and W. A. Brand, Rapid Communications in Mass Spectrometry **15**, 501 (2001).

[5] J. Worden, D. Noone, and K. Bowman, Nature **445**, 528 (2007).

[6] R. A. Berner, S. T. Petsch, J. A. Lake, D. J. Beerling, B. N. Popp, R. S. Lane, E. A. Laws, M. B. Westley, N. Cassar, F. I. Woodward, and W. P. Quick, Science (80-.). **287**, 1630 (2000).

[7] G. J. Martin, C. Guillou, M. L. Martin, M. T. Cabanis, Y. Tep, and J. Aerny, J. Agric. Food Chem. **36**, 316 (1988).

[8] J. Vanícek and W. H. Miller, J. Chem. Phys. **127**, 114309 (2007).

[9] H. C. Urey, J. Chem. Soc. , 562 (1947).

[10] M. Ceriotti and T. E. Markland, J. Chem. Phys. **138**, 014112 (2013).

[11] M. a. Webb and T. F. Miller, J. Phys. Chem. A **118**, 467 (2014).

[12] R. P. Feynman and A. R. Hibbs, *Quantum Mechanics and Path Integrals* (McGraw-Hill, New York, 1964).

[13] D. Chandler and P. G. Wolynes, J. Chem. Phys. **74**, 4078 (1981).

[14] M. Parrinello and A. Rahman, J. Chem. Phys. **80**, 860 (1984).

[15] M. Ceriotti and D. E. Manolopoulos, Phys. Rev. Lett. **109**, 100604 (2012).

[16] M. Buchowiecki and J. Vanícek, Chem. Phys. Lett. **588**, 11 (2013).

[17] O. Marsalek, P.-Y. Chen, R. Dupuis, M. Benoit, M. Méheut, Z. Bačić, and M. E. Tuckerman, J. Chem. Theory Comput. **10**, 1440 (2014).

[18] M. Ceriotti, G. a. R. Brain, O. Riordan, and D. E. Manolopoulos, Proc. R. Soc. A Math. Phys. Eng. Sci. **468**, 2 (2011).

[19] T. M. Yamamoto, J. Chem. Phys. **123**, 104101 (2005).

[20] M. Takahashi and M. Imada, Journal of the Physical Society of Japan **53**, 3765 (1984).

[21] L. Wang, M. Ceriotti, and T. E. Markland, J. Chem. Phys. **141**, 104502 (2014).

[22] D. Marx, M. E. Tuckerman, J. Hutter, and M. Parrinello, Nature **397**, 601 (1999).

[23] A. Hassanali, M. K. Prakash, H. Eshet, and M. Parrinello, Proc. Natl. Acad. Sci. USA U. S. A. **108**, 20410 (2011).

[24] L. I. Yeh, M. Okumura, J. D. Myers, J. M. Price, and Y. T. Lee, The Journal of Chemical Physics **91**, 7319 (1989).

[25] T. L. Guasco, M. A. Johnson, and A. B. McCoy, The Journal of Physical Chemistry A **115**, 5847 (2011).

[26] K. R. Asmis, N. L. Pivonka, G. Santambrogio, M. Brmmer, C. Kaposta, D. M. Neumark, and L. Wste, Science **299**, 1375 (2003).

[27] N. I. Hammer, E. G. Diken, J. R. Roscioli, M. A. Johnson, E. M. Myshakin, K. D. Jordan, A. B. McCoy, X. Huang, J. M. Bowman, and S. Carter, The Journal of Chemical Physics **122**, 244301 (2005).

[28] T. D. Fridgen, T. B. McMahon, L. MacAleese, J. Lemaire, and P. Maitre, The Journal of Physical Chemistry A **108**, 9008 (2004).

[29] F. Agostini, R. Vuilleumier, and G. Ciccotti, The Journal of Chemical Physics **134**, 084302 (2011).

[30] M. Park, I. Shin, N. J. Singh, and K. S. Kim, The Journal of Physical Chemistry A **111**, 10692 (2007).

[31] M. V. Vener, O. Kuhn, and J. Sauer, The Journal of Chemical Physics **114**, 240 (2001).

[32] J. Sauer and J. Döbler, ChemPhysChem **6**, 1706 (2005).

[33] H.-P. Cheng and J. L. Krause, The Journal of Chemical Physics **107**, 8461 (1997).

[34] O. Vendrell, F. Gatti, and H.-D. Meyer, The Journal of Chemical Physics **127**, 184303 (2007).

[35] M. Baer, D. Marx, and G. Mathias, Angewandte Chemie International Edition **49**, 7346 (2010).

[36] M. Kaledin, A. L. Kaledin, J. M. Bowman, J. Ding, and K. D. Jordan, The Journal of Physical Chemistry A **113**, 7671 (2009).

[37] X. Huang, B. J. Braams, and J. M. Bowman, The Journal of Chemical Physics **122**, 044308 (2005).

[38] E. S. Stoyanov, I. V. Stoyanova, and C. A. Reed, Journal of the American Chemical Society **132**, 1484 (2010).

[39] S. Olesen, T. Guasco, J. Roscioli, and M. Johnson, Chemical Physics Letters **509**, 89 (2011).

[40] J. Devlin, M. Severson, F. Mohamed, J. Sadlej, V. Buch, and M. Parrinello, Chemical Physics Letters **408**, 439 (2005).

[41] L. R. McCunn, J. R. Roscioli, M. A. Johnson, and A. B. McCoy, The journal of physical chemistry. B **112**, 321 (2008).

[42] M. Ceriotti, J. More, and D. E. Manolopoulos, Comput. Phys. Commun. **185**, 1019 (2014).

[43] M. Ceriotti, M. Parrinello, T. E. Markland, and D. E. Manolopoulos, J. Chem. Phys. **133**, 124104 (2010).

[44] J. M. Eiler, Earth and Planetary Science Letters **262**, 309 (2007).

[45] H. Craig, Geochimica et Cosmochimica Acta **3**, 53 (1953).

[46] C. Clayton, Marine and Petroleum Geology **8**, 232 (1991).

[47] B. Morasch, H. H. Richnow, B. Schink, and R. U. Meckenstock, Applied and Environmental Microbiology **67**, 4842 (2001).

[48] A. L. Sessions, T. W. Burgoyne, A. Schimmelmann, and J. M. Hayes, Organic Geochemistry **30**, 1193 (1999).

[49] G. D. Farguhar, J. R. Ehleringer, and K. T. Hubrick, Annual review of plant physiology **40**, 503.

[50] J. Hayes, K. H. Freeman, B. N. Popp, and C. H. Hoham, Organic Geochemistry **16**, 1115 (1990).

[51] K. H. Freeman, J. M. Hayes, J. M. Trendel, and P. Albrecht, Nature **343**, 254 (1990).

[52] L. Lindsay and D. a. Broido, Phys. Rev. B **81**, 205441 (2010).
[53] S. J. Stuart, A. B. Tutein, and J. A. Harrison, The Journal of Chemical Physics **112** (2000).
[54] D. J. Earl and M. W. Deem, Phys. Chem. Chem. Phys. **7**, 3910 (2005).
[55] T. J. Lee, J. M. Martin, and P. R. Taylor, The Journal of chemical physics **102**, 254 (1995).
[56] K. Vanommeslaeghe, E. Hatcher, C. Acharya, S. Kundu, S. Zhong, J. Shim, E. Darian, O. Guvench, P. Lopes, and I. Vorobyov, Journal of computational chemistry **31**, 671 (2010).
[57] T. E. Markland and B. J. Berne, Proc. Natl. Acad. Sci. USA **109**, 7988 (2012).
[58] P. E. Videla, P. J. Rossky, and D. Laria, J. Phys. Chem. Lett. **5**, 2375 (2014).
[59] S. Plimpton, J. Comput. Phys. **117**, 1 (1995).
[60] "CP2K," http://www.cp2k.org.
[61] V. Blum, R. Gehrke, F. Hanke, P. Havu, V. Havu, X. Ren, K. Reuter, and M. Scheffler, Comput. Phys. Commun. **180**, 2175 (2009).
[62] J. Liu, R. S. Andino, C. M. Miller, X. Chen, D. M. Wilkins, M. Ceriotti, and D. E. Manolopoulos, J. Phys. Chem. C **117**, 2944 (2013).
[63] A. Pérez and M. E. Tuckerman, J. Chem. Phys. **135**, 064104 (2011).